ISSN 1070-3284, Russian Journal of Coordination Chemistry, 2017, Vol. 43, No. 10, pp. 638–651. © Pleiades Publishing, Ltd., 2017.
Original Russian Text © O.A. Bredyuk, O.V. Loseva, A.V. Ivanov, V. Gowda, O.N. Antzutkin, 2017, published in Koordinatsionnaya Khimiya, 2017, Vol. 43, No. 10, pp. 602–616.

Three-Dimensional Polymeric Thallium(I) Morpholinedithiocarbamate $[Tl_2\{S_2CN(CH_2)_4O\}_2]_n$ and Its Capability of Binding Gold(III) from Solutions: Chemisorption Synthesis of a Heteronuclear Gold(III)–Thallium(III) Complex of the Ionic Type, $([Au\{S_2CN(CH_2)_4O\}_2][TlCl_4])_n$, the Role of Secondary Interactions Tl···O, Tl···S, and Au···S in the Supramolecular Self-Organization, ^{13}C MAS NMR, and Thermal Behavior

O. A. Bredyuk[a], O. V. Loseva[a], A. V. Ivanov[a, *], V. Gowda[b, c], and O. N. Antzutkin[b, d]

[a] *Institute of Geology and Nature Management, Far East Branch, Russian Academy of Sciences, Relochnyi per. 1, Blagoveshchensk, 675000 Russia*

[b] *Luleå University of Technology, SE-97187 Luleå, Sweden*

[c] *University of Oulu, P.O. Box 3000, FI-90014 Oulu, Finland*

[d] *Warwick University, Coventry CV4 7AL, UK*

**e-mail: alexander.v.ivanov@chemist.com*

Received May 8, 2017

Abstract—Crystalline polymeric thallium(I) morpholinedithiocarbamate $[Tl_2\{S_2CN(CH_2)_4O\}_2]_n$ (**I**) and the heteronuclear ion–polymeric gold(III)–thalium(III) complex $([Au\{S_2CN(CH_2)_4O\}_2][TlCl_4])_n$ (**II**) are preparatively isolated and characterized by X-ray diffraction analysis and ^{13}C MAS NMR spectroscopy. According to the X-ray diffraction data, the main structural units of compounds **I** and **II** (CIF files CCDC 1548079 and 1548080) are presented by the binuclear centrosymmetric molecule $[Tl_2\{S_2CN(CH_2)_4O\}_2]$, noncentrosymmetric complex cation $[Au\{S_2CN(CH_2)_4O\}_2]^+$, and isomeric complex anions $[TlCl_4]^-$. The formation of the three-dimensional polymeric structure (coordination number of Tl is 7), which is not characteristic of thallium(I) dithiocarbamates, is a consequence of the participation of the secondary Tl···O and Tl···S bonds of two types in the supramolecular self-organization of compound **I**. Nonequivalent secondary interactions of the first type join the binuclear molecules $[Tl_2\{S_2CN(CH_2)_4O\}_2]$ into polymer layers, which, in turn, form the three-dimensional polymeric framework due to the secondary bonds Tl···S. The revealed ability of freshly precipitated compound **I** to the chemisorption of gold(III) from solutions (2 M HCl) makes it possible to obtain heteronuclear supramolecular complex **II** as an individual form of binding. In the structure of the latter, the pairs of stronger secondary Au···S bonds join the gold(III) cations into dimers $[Au_2\{S_2CN(CH_2)_4O\}_4]^{2+}$ of the angular structure, the structural ordering of which is achieved in the cation-cationic polymeric chain $([Au_2\{S_2CN(CH_2)_4O\}_4]^{2+})_n$ of the helical type involving the pairs of less strong Au···S bonds between the adjacent binuclear units. The distorted tetrahedral anions $[TlCl_4]^-$ are localized between the polymeric chains. The study of the thermal behavior of compounds **I** and **II** by simultaneous thermal analysis makes it possible to establish the character of thermal transformations of the substances and to identify Tl_2S (**I**), TlCl, and elemental gold (**II**) as thermolysis products.

Keywords: three-dimensional polymeric thallium(I) alkylenedithiocarbamates, chemisorption binding of gold from solutions, heteronuclear gold(III)–thallium(III) dithiocarbamato-chlorido complexes, secondary interactions and self-organization of supramolecular structures, X-ray diffraction analysis, ^{13}C MAS NMR, simultaneous thermal analysis

DOI: 10.1134/S1070328417100013

INTRODUCTION

Thallium and its compounds are applied in various areas of practical activity: as semiconductors, catalysts, dyes, and pigments, as well as in nuclear medicine [1, 2]. Interest in thallium dithiocarbamates is evoked by their unusually complicated supramolecular

structures stabilized by secondary interactions of different types [3–9] and by the possibility of practical use as precursors of various film and nanosized thallium sulfides [10–17]. An enhanced reactivity of highly dispersed thallium dithiocarbamates caused by a significant total concentration of coordinately unsaturated centers of sulfur and thallium in the developed surface layer indicates the possibility of their use as efficient chemisorbents of metal ions from solutions.

Polynuclear thallium(I) *N,N-cyclo*-pentamethylene- [18, 19] and *N,N-cyclo*-hexamethylenedithiocarbamates [20] studied by us earlier are characterized by two-dimensional polymeric supramolecular structures in the formation of which the secondary Tl···S bonds play the determining role. The study of the chemisorption activity of thallium(I) dialkyldithiocarbamates $[Tl_2(S_2CNR_2)_2]_n$ (R = CH_3, C_2H_5, *iso*-C_4H_9) including linear and branched substituents toward solutions of gold(III) in 2 M HCl made it possible to obtain and characterize in detail ion–polymeric heteronuclear gold(III)–thallium(III) complexes $[Au_2\{S_2CN(CH_3)_2\}_4][TlCl_4]_2$ and $([Au(S_2CNR_2)_2][TlCl_4])_n$ (R = C_2H_5, *iso*-C_4H_9) [21, 22]. Therefore, it seemed interesting to study the ability of thallium(I) morpholinedithiocarbamate (MfDtc), whose ligand contains the heterocyclic fragment, to bind gold(III) from solutions.

Polymeric bis[μ_2-(morpholinedithiocarbamato-*S,S,S',S'*)]dithallium(I) $[Tl_2\{S_2CN(CH_2)_4O\}_2]_n$ (**I**), the first representative of thallium(I) dithiocarbamate complexes with the three-dimensional polymeric structure, was obtained in this work. The role of the secondary Tl···O and Tl···S interactions in the supramolecular self-organization of compound **I** was shown, and its reactivity toward $[AuCl_4]^-$/2 M HCl was studied. The formation of ion–polymeric bis(morpholinedithiocarbamato-*S,S'*)gold(III) tetrachlorothallate(III) $([Au\{S_2CN(CH_2)_4O\}_2][TlCl_4])_n$ (**II**) was established by the results of the chemisorption binding of gold(III) and the accompanying redox process. The supramolecular structures of preparatively isolated crystalline compounds **I** and **II** were characterized in detail by the X-ray diffraction and ^{13}C MAS NMR data. The thermal behavior and conditions for the regeneration of bound gold(III) were studied by simultaneous thermal analysis (STA).

EXPERIMENTAL

Sodium morpholinedithiocarbamate was obtained by the reaction of carbon bisulfide (Merck) and morpholine (Aldrich) in an alkaline medium [23]. The starting salt was additionally characterized by the ^{13}C MAS NMR spectroscopy:

for $Na\{S_2CN(CH_2)_4O\} \cdot 2H_2O$ (δ, ppm):
204.8 (=NC(S)S–); 67.6, 67.2 (–OCH_2–); 54.6, 53.9, 53.5 (=NCH_2–).

Synthesis of compound I was carried out by the reaction of a solution of $TlNO_3$ (Merck) (0.0727 g, 0.2729 mmol) in water (10 mL) with a solution of $Na\{S_2CN(CH_2)_4O\} \cdot 2H_2O$ (0.0604 g, 0.2729 mmol) in water (10 mL). The white bulky precipitate was filtered off, washed with water, and dried in air. The yield was 78%. To obtain single crystals, the complex was dissolved in boiling *N,N*-dimethylformamide (~153°C). Colorless transparent crystals were formed immediately on cooling the solution. For further experiments, cubic crystals of compound **I** were taken from the mother liquor and dried on a filter.

The chemisorption synthesis of compound **II** was based on binding $AuCl_3$ from a solution in 2 M HCl with freshly precipitated thallium(I) morpholinedithiocarbamate $[Tl_2\{S_2CN(CH_2)_4O\}_2]_n$, being a bulky microcrystalline white precipitate. The interaction of the precipitate with a solution of $H[AuCl_4]$ results in a change in the color to yellow already at the first minutes with the simultaneous decoloration of the working solution. The degree of binding gold from the solution to the solid phase (98.3%) indicates the formation of new compounds in the studied system. The heterogeneous reaction of gold(III) binding to the solid phase includes the partial ion exchange and redox process:

$$3[Tl_2\{S_2CN(CH_2)_4O\}_2] + 5H[AuCl_4] = 3[Au\{S_2CN(CH_2)_4O\}_2][TlCl_4] + 3TlCl + 2Au + 5HCl.$$

A solution of $AuCl_3$ (10 mL) in 2M hydrochloric acid containing 44.5 mg of gold was poured to complex **I** (100 mg), and the mixture was stirred for 1 h. The residual content of gold in the solution was determined on a Hitachi atomic absorption spectrometer (1 class, model 180-50). The obtained yellow precipitate was filtered off, washed with water, dried on a filter, and dissolved in acetone on heating. Transparent crystals of compound **II** (yellow needles) for diffraction analysis were obtained by the slow evaporation of the solvent at room temperature.

^{13}C MAS NMR data (δ, ppm) for $[Tl_2\{S_2CN(CH_2)_4O\}_2]_n$ (**I**): 205.2 (=NC(S)S–); 67.2 (–OCH_2–); 51.0, 49.7 (1 : 1, =NCH_2–); for $([Au\{S_2CN(CH_2)_4O\}_2][TlCl_4])_n$ (**II**): 198.6, 194.3 (1 : 1, =NC(S)S–); 67.0, 66.0, 65.0 (2 : 1 : 1, –OCH_2–); 51.4, 49.2, 48.7 (2 : 1 : 1, =NCH_2–).

^{13}C MAS NMR spectra were recorded on an Ascend Aeon spectrometer (Bruker) with a working frequency of 100.64 MHz (for ^{13}C), a superconducting magnet (B_0 = 9.4 T) with the closed condensation cycle of helium through an external compressor, and the Fourier transform. Proton cross polarization and the decoupling effect for the suppression of $^{13}C-^{1}H$ interactions using a radiofrequency field at the resonance frequency of protons were applied [24]. Samples of complexes **I** and **II** (~50 or 80 mg, respectively)

were placed in a 4.0-mm ceramic rotor of ZrO_2. The rotation of a sample at the magic angle and a frequency of 10 000(1) Hz was used in ^{13}C MAS NMR measurements and 10240 or 1320 signal transients were accumulated, with a duration of proton $\pi/2$ pulses of 2.7 μs, a contact time $^1H-^{13}C$ of 3.0 ms, and a pulse delay of 5.0 or 3.0 s. Isotropic chemical shifts ($\delta(^{13}C)$, ppm) are given relative to one of the components of crystalline adamantane used as an external standard ($\delta = 38.48$ ppm relative to tetramethylsilane) with a correction applied to the drift of the magnetic field strength, whose frequency equivalent was 0.025 Hz/h.

X-ray diffraction analysis. Single crystals of compounds **I** and **II** were fixed at the end of a glass capillary with the epoxide resin. Experiments were carried out on a Bruker-Nonius X8 Apex CCD diffractometer (MoK_α radiation, $\lambda = 0.71073$ Å, graphite monochromator) at 150(2) K. The data were collected using a standard procedure: φ and ω scanning of narrow frames. An absorption correction was applied empirically using the SADABS program [25]. The structures were determined by a direct method and refined by least squares (for F^2) in the full-matrix anisotropic approximation of non-hydrogen atoms. The positions of hydrogen atoms were calculated geometrically and included into the refinement by the riding model. The calculations on structure determination and refinement were performed using the SHELXTL program package [25]. The main crystallographic data and results of structure refinement are presented in Table 1. Selected bond lengths and angles are given in Table 2.

The coordinates of atoms, bond lengths, and angles were deposited with the Cambridge Crystallographic Data Centre (CIF files CCDC 1548079 (**I**) and 1548080 (**II**); deposit@ccdc.cam.ac.uk or http://www.ccdc.cam.ac.uk).

Thermal behavior of compounds **I** and **II** was studied by the STA method with the simultaneous detection of thermogravimetry (TG) and differential scanning calorimetry (DSC) curves. The study was carried out on an STA 449C Jupiter instrument (NETZSCH) in corundum crucibles under caps with a hole providing a vapor pressure of 1 atm in the course of the thermal decomposition of the sample. The heating rate was 5°C/min to 455 and 1100°C in an argon atmosphere. The limiting heating temperature for compound **I** was chosen by the fact that Tl_2S melts at 449 or 452°C (depending on the method of preparation) [26]. The weight of the samples was 3.466–9.594 (**I**) and 2.787–10.511 mg (**II**), the accuracy of temperature measurements was ±0.4°C, and the weight change was $\pm 1 \times 10^{-4}$ mg. When recording TG and DSC curves, the correction file was used, as well as calibrations by temperature and sensitivity for a specified temperature program and heating rate. The melting points of compounds **I** and **II** were determined independently with a PTP(M) instrument (OAO Khimlaborpribor, Russia).

RESULTS AND DISCUSSION

The ^{13}C MAS NMR spectra of complexes **I** and **II** contain resonance signals of the =NC(S)S–, $-OCH_2-$, and $=NCH_2-$ groups (Fig. 1). The dithiocarbamate groups most sensitive to the structural state of the MfDtc ligands are presented in the experimental spectra by one or two (1 : 1) ^{13}C resonance signals. It is clear from this that in compound **I** the ligands are structurally unified, whereas the structure of compound **II** contains two groups of nonequivalent MfDtc ligands. Note that heteronuclear complex **II** is characterized by significantly lower (compared to the starting polymeric complex **I**) ^{13}C chemical shifts of the =NC(S)S– groups (see the syntheses of compounds **I** and **II**). The revealed decrease (by 6.6 and 10.9 ppm) in the discussed values of $\delta(^{13}C)$ indicates the complete redistribution of the MfDtc ligands in the internal sphere of gold(III), whose electron density is involved more efficiently in the additional shielding of the carbon rings of the dithiocarbamate groups. In the small-sized four-membered rings $[AuS_2C]$, the positions of the oppositely lying gold and carbon atoms are substantially approached, indicating *trans*-annular interactions between them.

The structural organization of the synthesized complexes was established by X-ray diffraction analysis. Before discussing the structures of compounds **I/II**, let us consider the general features of the MfDtc ligands. The N–C(S)S bonds are shorter (1.344/1.309, 1.293 Å) than those of $N-CH_2$ (1.462, 1.468/1.45–1.490 Å), which indicates a considerable contribution of double bonding to the formally ordinary bond (and admixing of the sp^2-hybrid state to the sp^3-hybrid state of the nitrogen and carbon atoms) due to the mesomeric effect of the =NC(S)S– groups. Not quite coplanar (due to the peripheral carbon atoms) mutual arrangement of atoms in the structural C_2NCS_2 groups is illustrated by the torsion angles S–C–N–C, the deviation of which from 0° or 180° does not exceed 6.3° and 7.9°, respectively (Table 2). The six-membered heterocyclic $-N(CH_2)_4O$ fragments in the chair conformation are *trans*-oriented relative to the equatorial plane of the octahedral molecule $[Tl_2\{S_2CN(CH_2)_4O\}_2]$. On the contrary, in the complex cations $[Au\{S_2CN(CH_2)_4O\}_2]^+$, the discussed cyclic groups exist in the *cis*-position relative to the plane of the $[AuS_4]$ chromophore. The bond angles in the heterocycles of the MfDtc ligands in the complexes **I** and **II** mainly exceed the ideal tetrahedral value and range from 109.5° to 112.8° and from 108.9° to 119.7°, and the C–O bond lengths are 1.1.427(6), 1.432(7)/1.390(9)–1.436(11) Å, respectively.

Table 1. Crystallographic data and experimental and refinement parameters for the structures of compounds $[Tl_2\{S_2CN(CH_2)_4O\}_2]_n$ (**I**) and $([Au\{S_2CN(CH_2)_4O\}_2][TlCl_4])_n$ (**II**)

Parameter	Value	
	I	**II**
Empirical formula	$C_{10}H_{16}N_2O_2S_4Tl_2$	$C_{10}H_{16}N_2O_2S_4Cl_4AuTl$
FW	733.23	867.62
Crystal system	Triclinic	Orthorhombic
Space group	$P\bar{1}$	*Pnna*
a, Å	6.5260(8)	15.3384(10)
b, Å	8.4243(7)	13.2260(6)
c, Å	8.8900(8)	21.8178(14)
α, deg	66.529(4)	
β, deg	83.685(5)	
γ, deg	67.550(4)	
V, Å^3	413.82(7)	4426.1(5)
Z	1	8
ρ_{calcd}, g/cm^3	2.942	2.604
μ, mm^{-1}	19.950	14.761
F(000)	332	3184
Crystal size, mm	0.12 × 0.10 × 0.05	0.30 × 0.04 × 0.04
Range of data collection over θ, deg	2.84–27.50	1.80–27.53
Ranges of reflection indices	$-8 \le h \le 5$, $-10 \le k \le 10$, $-11 \le l \le 11$	$-19 \le h \le 14$, $-15 \le k \le 17$, $-28 \le l \le 24$
Measured reflections	3314	15 955
Independent reflections	1880 (R_{int} = 0.0308)	5098 (R_{int} = 0.0646)
Reflections with $I > 2\sigma(I)$	1748	3164
Refinement variables	91	245
GOOF	1.039	0.999
R factors for $F^2 > 2\sigma(F^2)$	R_1 = 0.0264, wR_2 = 0.0570	R_1 = 0.0488, wR_2 = 0.1010
R factors for all reflections	R_1 = 0.0296, wR_2 = 0.0579	R_1 = 0.0997, wR_2 = 0.1128
Residual electron density (min/max), *e*/Å^3	−1.483/1.196	−2.231/1.973

Table 2. Selected bond lengths (*d*), bond angles (ω), and torsion angles (φ) in compounds **I** and **II***

I

Bond	*d*, Å	Bond	*d*, Å
Tl(1)–S(1)	3.0148(13)	Tl(1)···O(1)^{d}	3.112(4)
Tl(1)–S(1)^{a}	3.1042(14)	S(1)–C(1)	1.729(6)
Tl(1)–S(2)	3.3472(15)	S(2)–C(1)	1.716(5)
Tl(1)–S(2)^{a}	3.0775(13)	N(1)–C(1)	1.344(6)
Tl(1)···S(2)^{b}	3.6873(15)	N(1)–C(2)	1.468(6)
Tl(1)···O(1)^{c}	3.175(4)	N(1)–C(4)	1.462(6)
Angle	**ω, deg**	**Angle**	**ω, deg**
S(1)Tl(1)S(2)	55.30(3)	O(1)^{c}Tl(1)S(2)^{b}	94.50(7)
S(1)Tl(1)S(1)^{a}	104.47(3)	O(1)^{d}Tl(1)S(1)	161.23(8)
S(1)Tl(1)S(2)^{a}	83.78(3)	O(1)^{d}Tl(1)S(2)	143.36(7)
S(1)Tl(1)S(2)^{b}	81.07(3)	O(1)^{d}Tl(1)S(1)^{a}	85.68(8)
S(2)Tl(1)S(1)^{a}	78.09(3)	O(1)^{d}Tl(1)S(2)^{a}	88.78(7)
S(2)Tl(1)S(2)^{a}	108.77(3)	O(1)^{d}Tl(1)S(2)^{b}	80.17(7)
S(2)Tl(1)S(2)^{b}	136.11(4)	O(1)^{c}Tl(1)O(1)^{d}	80.65(10)
S(1)^{a}Tl(1)S(2)^{a}	57.36(4)	Tl(1)S(1)C(1)	91.59(17)
S(1)^{a}Tl(1)S(2)^{b}	122.05(3)	Tl(1)S(2)C(1)	81.08(18)
S(2)^{a}Tl(1)S(2)^{b}	66.38(4)	Tl(1)^{a}S(1)C(1)	84.31(17)
O(1)^{c}Tl(1)S(1)	100.78(7)	Tl(1)^{a}S(2)C(1)	85.36(17)
O(1)^{c}Tl(1)S(2)	89.76(7)	Tl(1)S(1)Tl(1)^{a}	75.52(3)
O(1)^{c}Tl(1)S(1)^{a}	138.00(7)	Tl(1)S(2)Tl(1)^{a}	71.23(3)
O(1)^{c}Tl(1)S(2)^{a}	159.61(8)	S(1)C(1)S(2)	119.0(3)
Angle	**φ, deg**	**Angle**	**φ, deg**
Tl(1)S(1)S(2)C(1)	138.3(4)	S(1)C(1)N(1)C(2)	–6.3(7)
Tl(1)^{a}S(1)S(2)C(1)	–136.5(4)	S(1)C(1)N(1)C(4)	–176.3(4)
S(1)Tl(1)C(1)S(2)	144.9(3)	S(2)C(1)N(1)C(2)	174.1(4)
S(1)Tl(1)^{a}C(1)S(2)	–144.2(3)	S(2)C(1)N(1)C(4)	4.1(7)

II

Bond	*d*, Å	Bond	*d*, Å
Cation			
Au(1)–S(1)	2.331(3)	S(3)–C(6)	1.742(10)
Au(1)–S(2)	2.337(3)	S(4)–C(6)	1.711(11)
Au(1)–S(3)	2.332(3)	N(1)–C(1)	1.293(14)
Au(1)–S(4)	2.330(3)	N(1)–C(2)	1.45(2)
Au(1)···S(2)^{a}	3.576(3)	N(1)–C(5)	1.49(2)
Au(1)···S(4)^{b}	3.559(3)	N(2)–C(6)	1.309(12)
S(1)–C(1)	1.718(12)	N(2)–C(7)	1.490(13)
S(2)–C(1)	1.725(12)	N(2)–C(10)	1.474(12)

Table 2. (Contd.)

Anions			
Tl(1)–Cl(1)	2.418(2)	Tl(1)–Cl(2)	2.443(3)
Tl(2A)–Cl(3)	2.447(4)	Tl(2B)–Cl(3)[d]	2.371(5)
Tl(2A)–Cl(4)	2.390(8)	Tl(2B)–Cl(5)	2.46(2)
Tl(2B)–Cl(3)	2.302(5)	Tl(2B)–Cl(6)	2.49(2)
Angle	ω, deg	Angle	ω, deg
Cation			
S(1)Au(1)S(2)	75.57(11)	Au(1)S(1)C(1)	86.2(4)
S(1)Au(1)S(3)	104.62(10)	Au(1)S(2)C(1)	85.8(4)
S(1)Au(1)S(4)	179.53(10)	Au(1)S(3)C(6)	85.4(4)
S(2)Au(1)S(3)	176.38(9)	Au(1)S(4)C(6)	86.2(3)
S(2)Au(1)S(4)	104.02(10)	S(1)C(1)S(2)	112.3(6)
S(3)Au(1)S(4)	75.80(9)	S(3)C(6)S(4)	112.1(6)
Anions			
Cl(1)Tl(1)Cl(2)	103.22(9)	Cl(1)Tl(1)Cl(2)[c]	107.15(10)
Cl(1)Tl(1)Cl(1)[c]	130.58(12)	Cl(2)Tl(1)Cl(2)[c]	102.47(13)
Cl(3)Tl(2A)Cl(4)	114.0(3)	Cl(3)Tl(2B)Cl(6)	106.4(6)
Cl(3)Tl(2A)Cl(3)[d]	101.3(2)	Cl(3)Tl(2B)Cl(3)[d]	108.1(2)
Cl(3)Tl(2A)Cl(4)[d]	111.5(3)	Cl(5)Tl(2B)Cl(6)	108.9(9)
Cl(4)Tl(2A)Cl(4)[d]	104.9(6)	Cl(5)Tl(2B)Cl(3)[d]	114.9(6)
Cl(3)Tl(2B)Cl(5)	112.3(6)	Cl(6)Tl(2B)Cl(3)[d]	105.7(6)
Angle	φ, deg	Angle	φ, deg
Cation			
Au(1)S(1)S(2)C(1)	178.3(7)	S(2)C(1)N(1)C(2)	–176.3(12)
Au(1)S(3)S(4)C(6)	171.4(6)	S(2)C(1)N(1)C(5)	–7.9(18)
S(1)Au(1)C(1)S(2)	178.5(6)	S(3)C(6)N(2)C(7)	–5.0(13)
S(3)Au(1)C(6)S(4)	172.4(5)	S(3)C(6)N(2)C(10)	–175.6(7)
S(1)C(1)N(1)C(2)	3.7(18)	S(4)C(6)N(2)C(7)	172.2(7)
S(1)C(1)N(1)C(5)	172.1(11)	S(4)C(6)N(2)C(10)	1.5(13)

* Symmetry transforms: [a] $-x, 1-y, -z$; [b] $1+x, y, z$; [c] $-x, -y, 1-z$; [d] $1+x, y, z-1$ (**I**); [a] $1/2-x, 1-y, z$; [b] $x, 1/2-y, 3/2-z$; [c] $1/2-x, -y, z$; [d] $x, 1/2-y, 1/2-z$ (**II**).

The unit cell of compound **I** contains one centrosymmetric binuclear molecule $[Tl_2\{S_2CN(CH_2)_4O\}_2]$, which is the main structural unit of the complex, and the formation of the molecule involves two bridging dithiocarbamate ligands. The intradimer interatomic Tl–Tl distance is 3.748 Å (Figs. 2, 3a). Each thallium atom participating in the coordination of all the four sulfur atoms (of two dithio ligands) forms two stronger (Tl(1)–S(1) 3.015, Tl(1)–S(2)[a] 3.078 Å) and two weaker (Tl(1)–S(1)[a] 3.104, Tl(1)–S(2) 3.347 Å) bonds with the Dtc ligands. The binuclear molecule of complex **I** is octahedral. Four sulfur atoms form the rectangular equatorial plane with the sides S···S 2.967 Å (intraligand distance) and 4.068 Å (interligand distance) and the angles somewhat deviating from the right angle (85.36° and 94.64°), and the metal atoms occupy the axial positions. In addition, the octahedron discussed is distorted due to the compression along the Tl–Tl axis (its length is 3.748 Å; for comparison, the distances between the diagonally oriented sulfur atoms are 4.838 and 5.226 Å).

The positions of the thallium and carbon atoms of the =NC(S)S– groups in the structure of compound **I** are appreciably approached. The Tl–C interatomic

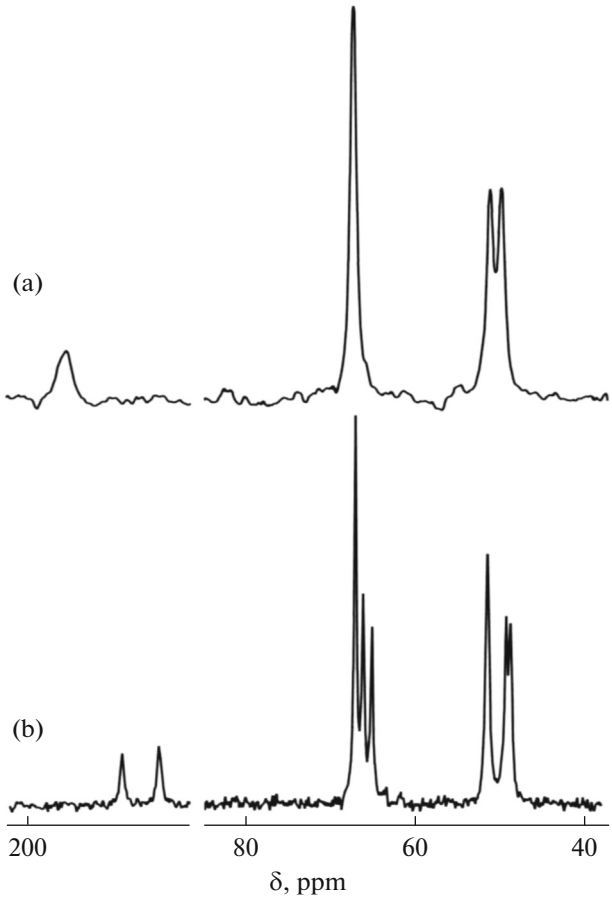

Fig. 1. ^{13}C MAS NMR spectra of complexes (a) **I** and (b) **II**. Scan number/rotation frequency (in kHz): 10 240/10 and 1310/10, respectively.

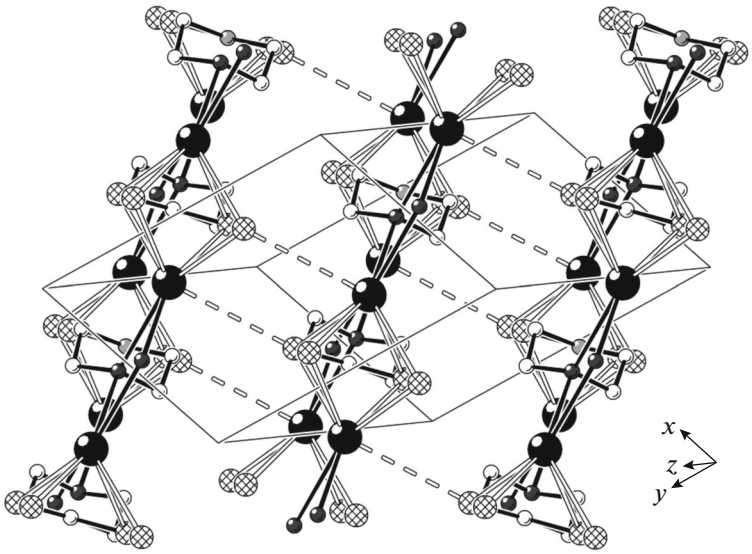

Fig. 2. Supramolecular crystal structure in compound **I**. Dashed lines show the secondary Tl···S bonds joining the polymer layers of the binuclear $[Tl_2\{S_2CN(CH_2)_4O\}_2]$ molecules into the three-dimensional polymeric framework.

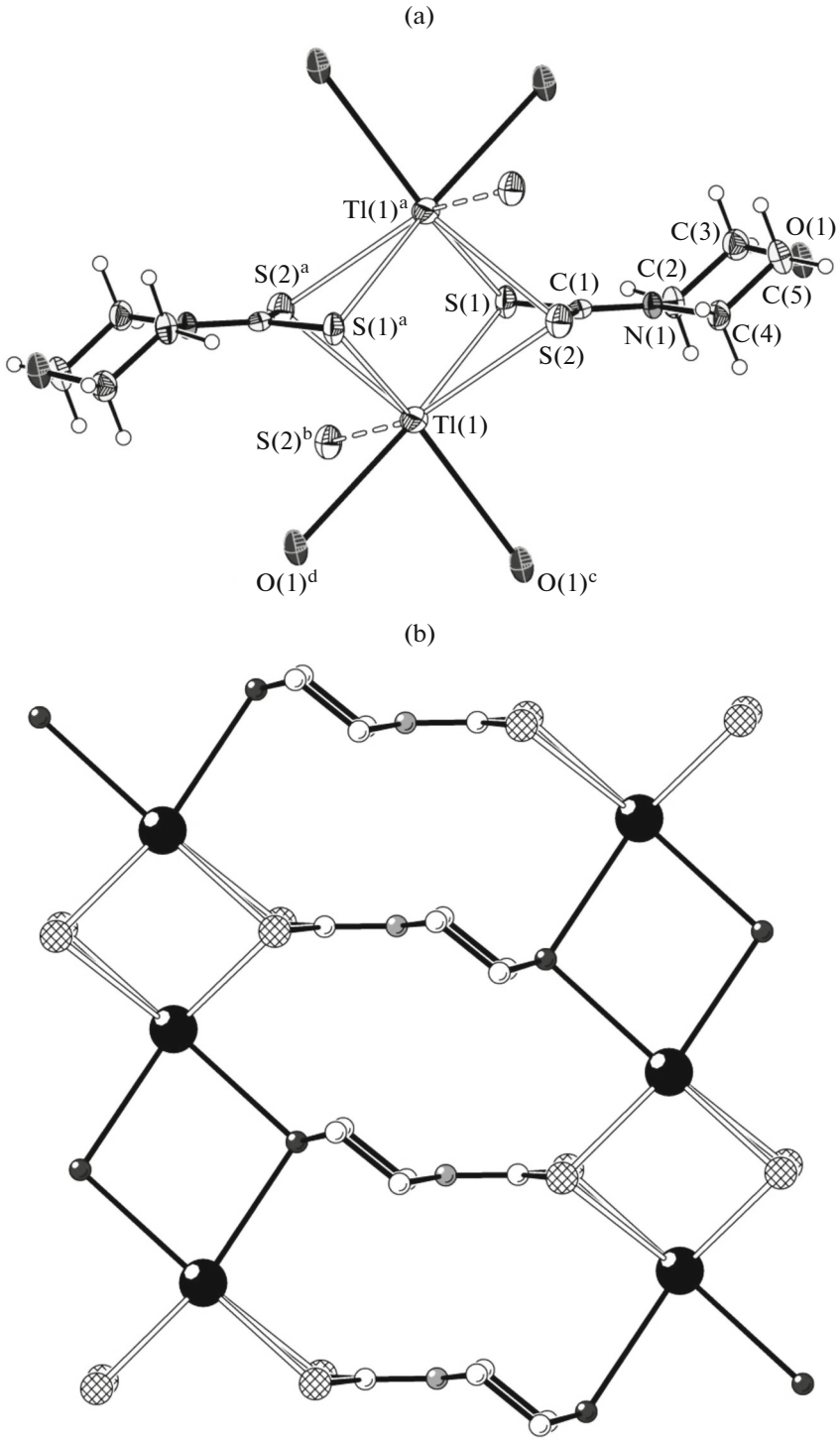

Fig. 3. Structure of the octahedral binuclear molecule $[Tl_2\{S_2CN(CH_2)_4O\}_2]$ with the vertex arrangement of the metal atoms (70% probability ellipsoids). (a) Secondary intermolecular Tl···S bonds shown by dashed lines and (b) the projection onto the [111] plane of the two-dimensional layer formed by the binuclear $[Tl_2\{S_2CN(CH_2)_4O\}_2]$ molecules due to the nonequivalent Tl···O secondary bonds.

distances are 3.40 and 3.52 Å (the sum of the van der Waals radii of the Tl and C atoms is 3.73 Å [27–29]). This is favored by a fairly large SCS angle (119.0°) and the inflection of the four-membered metallocycles $[TlS_2C]$ along the S–S axis (Fig. 3a): the angles between the planes of the [TlSS] and [CSS] half-cycles are 136.5° and 138.3°.

In the discussed binuclear molecules $[Tl_2\{S_2CN(CH_2)_4O\}_2]$, the coordination number of Tl is 4. It is known that thallium(I) is characterized by

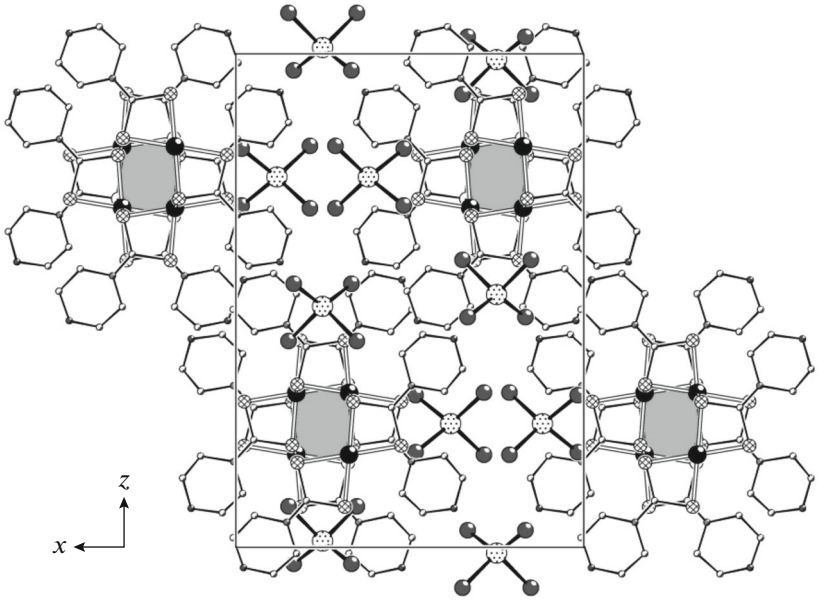

Fig. 4. Packing of structural units in the crystal of compound **II** (projection onto the plane *xz*). Positions of hollow channels inside the helical supramolecular chains $([Au_2\{S_2CN(CH_2)_4O\}_4]^{2+})_n$ are gray-colored.

high coordination numbers, in particular, they reach 5–7 in the dithiocarbamate complexes [3–20]. The discussed compound **I** is not exception, where the further coordination saturation of thallium occurs due to the oxygen atoms of the heterocyclic fragments. Each oxygen atom nonsymmetrically interacts with the thallium atoms of two adjacent binuclear molecules (Fig. 3b). The lengths of the secondary bonds[1] Tl···O are 3.112 and 3.175 Å (the sum of the van der Waals radii of the Tl and O is 3.48 Å [27–29]). In turn, each thallium atom additionally forms two nonequivalent secondary bonds with the oxygen atoms of two dithiocarbamate ligands increasing the coordination number of Tl to 6. Thus, a new type of secondary Tl···O interactions is observed in thallium(I) morpholinedithiocarbamate. These interactions link the binuclear molecules into polymeric chains (angle TlTlTl 164.02°, interdimer distance Tl–Tl 4.794 Å) that are combined into the two-dimensional polymer layer (Fig. 3b). The interaction between the layers accompanied by the formation of the three-dimensional framework occurs due to the secondary Tl···S bonds, which are additionally formed by the thallium atoms of each binuclear molecule with two adjacent layers (Fig. 2). The discussed interactions are relatively weak. Nevertheless, the Tl(1)···S(2)^b bond length is 3.687 Å, which is reliably shorter than the sum of the van der Waals radii of the Tl and S atoms (3.76 Å [27–29]). Thus, as in the earlier described thallium(I) dimethyldithiocarbamate [5], the overall coordination number of Tl in complex **I** is 7. The polyhedron of thallium is a distorted one-capped trigonal prism formed by five sulfur atoms and two oxygen atoms, and one S atom is located beyond the face of the prism [31].

The unit cell of complex **II** contains eight formula units (Fig. 4). In the noncentrosymmetric complex cation $[Au\{S_2CN(CH_2)_4O\}_2]^+$, the coordination mode of the MfDtc ligands that is close to S,S'-isobidentate (Au–S 2.330–2.337 Å; Fig. 5a, Table 2) results in the formation of the bicyclic system $[CS_2AuS_2C]$ including two four-membered metallocycles $[AuS_2C]$ with the common gold atom. In the small-sized cycles $[AuS_2C]$, the approached positions of the oppositely lying atoms reflect the interatomic distances Au–C 2.796, 2.803 and S–S 2.860, 2.864 Å (the sums of the van der Waals radii of the corresponding pairs of atoms are 3.36 and 3.60 Å, respectively [27–29]). This fact indicates the direct *trans*-annular interaction between the discussed pairs of atoms and a high concentration of the π-electron density inside the cycles. Some tetrahedral distortion is observed only in one of the $[AuS_2C]$ cycles, because the torsion angles Au(1)–S(3)–S(4)–C(6) and S(3)–Au(1)–C(6)–S(4) deviate from 180° by 8.6° and 7.6°, respectively (Table 2). The geometry of the chromophore $[AuS_4]$ is close to the planar tetragonal one, to which the low-spin intraorbital dsp^2-hybrid state of gold(II) corresponds (coordination number of Au is 4).

[1] The concept of secondary bonds was first proposed [30] for the description of interactions characterized by the distances comparable with the sums of the van der Waals radii of the corresponding atoms.

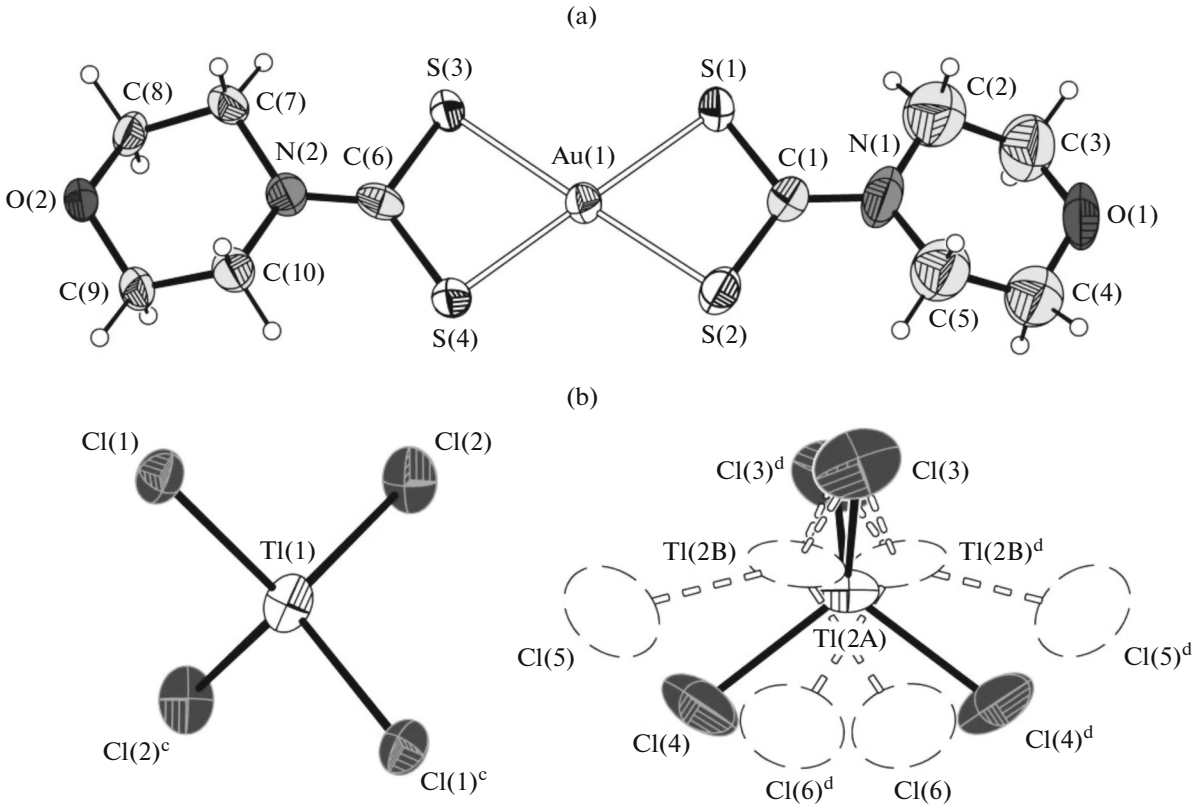

Fig. 5. (a) Structures of the complex cation $[Au\{S_2CN(CH_2)_4O\}_2]^+$ (50% probability ellipsoids) and (b) isomeric complex anions $[TlCl_4]^-$ of the Tl(1) and Tl(2) atoms (dashed lines show the structural positions of statistically distributed atoms in alternative orientations of the Tl(2) anion: populations of positions are 0.50 for A, 0.25 for B, and 0.25 for B^d; 50% probability ellipsoids).

The anionic moiety of complex **II** is presented by two structurally nonequivalent discrete tetrachlorothallate(III) ions (Fig. 5b) characterized by distorted tetrahedral structures (sp^3-hybrid state of the central thallium atoms). All ClTlCl bond angles deviate appreciably from the ideal tetrahedral value (101.3°–130.6°), and the Tl–Cl bond lengths range from 2.302 to 2.490 Å. The Tl–Cl bonds are nonequivalent in pairs in both anions discussed. The structural situation in the anions containing the Tl(2) atom is impeded by the fact that the thallium and chlorine atoms (Cl(4) and $Cl(4)^d$) are statistically distributed between three structural positions A, B, and B^d in a ratio of 0.50 : 0.25 : 0.25 (Fig. 5b, Table 2).

Owing to the pairs of the symmetric secondary bonds $Au(1)\cdots S(4)^b$ and $Au(1)^b\cdots S(4)$ (a distance of 3.559 Å somewhat exceeds the sum of the van der Waals radii of the sulfur and gold atoms equal to 3.46 Å [27–29]), the interaction between the adjacent gold(III) cations results in their joining into dimeric aggregates $[Au_2\{S_2CN(CH_2)_4O\}_4]^{2+}$ with the angular orientation of the mononuclear fragments and the planes of the $[AuS_4]$ chromophores retained parallel. It is seen from the projection on the plane *xz* that the mutual spatial orientation of the $[Au\{S_2CN(CH_2)_4O\}_2]^+$ cations is presented by the Г-shaped configuration: the bisector axes of the mononuclear cations passing through the CAuC atoms in the bicyclic fragments $[CS_2AuS_2C]$ form an angle of 95° on the projection (Fig. 6). In the discussed binuclear cation (Au–Au 4.331 Å), each gold atom exists in the environment of five sulfur atoms (configuration of an extended tetragonal pyramid). The pairs of the heterocyclic $N(CH_2)_4O$ fragments are characterized by the opposite spatial orientation relative to the planes of the $[AuS_4]$ chromophores due to interligand repulsion forces (Fig. 7).

In turn, each binuclear cation forms two pairs of less strong secondary Au···S bonds with the adjacent dimers ($Au(1)\cdots S(2)^a$ and $Au(1)^a\cdots S(2)$ 3.576 Å) (Fig. 7). Note that the S(2) atoms of the second MfDtc ligand participate in these secondary interactions and lie together with the S(4) atom at the same side of the central gold atom. The simultaneous participation in the secondary interactions of the S(4) and S(2) atoms *cis*-oriented in the $[AuS_4]$ chromophore leads to the "twisting" of the gold(III) cations to form the supramolecular cation-cationic chain $([Au_2\{S_2CN(CH_2)_4O\}_4]^{2+})_n$ of the helical type oriented toward the crystallographic axis *y*. Two binuclear cations $[Au_2\{S_2CN(CH_2)_4O\}_4]^{2+}$ (or four mononuclear cations $[Au\{S_2CN(CH_2)_4O\}_2]^+$) form the

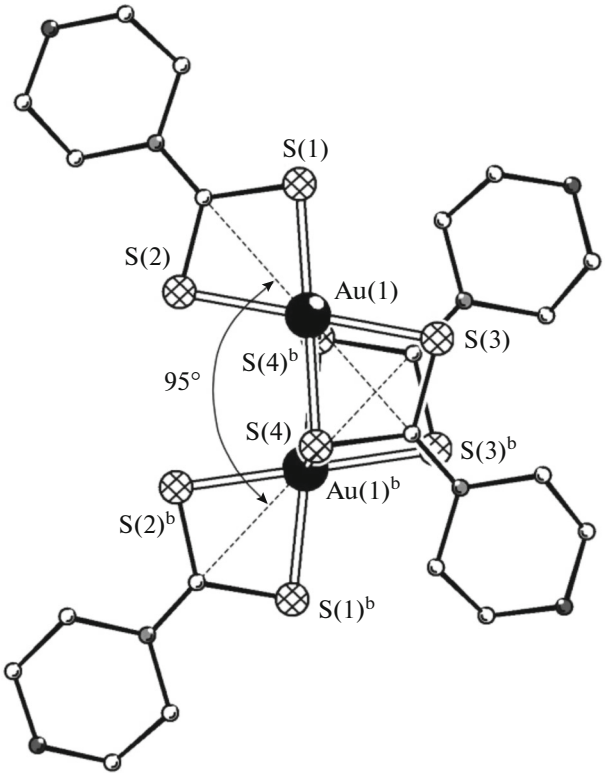

Fig. 6. Projection of the structure of the binuclear $[Au_2\{S_2CN(CH_2)_4O\}_4]^{2+}$ cation on the plane *xz*.

full coil of the helix, which looks as a four-leafed aggregate in the projection on the plane *xz* (Fig. 4). A hollow channel with a cross section of ~3.1 × 2.5 Å lies inside each helical chain (shown by gray in Fig. 4). In the chain discussed, each gold atom builds up its polyhedron to the extended octahedron $[AuS_6]$ (angle S···Au···S 177.70°) due to two secondary Au···S bonds. The interdimer Au–Au distance in the discussed chain is 3.993 Å, and the angle AuAuAu is 129.20°. In the projection on the plane *xz*, the bisector axes of the adjacent $[Au\{S_2CN(CH_2)_4O\}_2]^+$ cations of different binuclear cations form an angle of 85°. Structurally nonequivalent tetrachlorothallate(III) ions $[TlCl_4]^-$ participate in the spatial isolation of the supramolecular helical chains $([Au_2\{S_2CN(CH_2)_4O\}_4]^{2+})_n$ and are localized in the bulk between the chains.

The thermal behavior of complexes **I** and **II** was studied by the STA method with the detection of the TG and DSC curves. Compound **I** is thermally stable up to the melting point. A significant mass loss is detected in the TG curve (Fig. 8*a*) only after melting. As the temperature increases, the smooth mass loss transits to the steeply descending region of the TG curve (~290–350°C), showing an intense thermolysis of compound **I** with the formation of Tl_2S, being the final product of the thermal transformations of thallium(I) dithiocarbamates [17, 19]. The weight of the residue is 60.13% of the initial mass and corresponds to the calculated value (60.12%) for thallium(I) sulfide.

The DSC curve exhibits several thermal effects (Fig. 8*b*). The first intensive endothermic effect with an extreme at 264.5°C (extrapolated temperature 261.8°C) should be assigned to the melting of compound **I**. For independent determination in a glass capillary, the melting of the complex was established in the range of 262–264°C. The broadened asymmetric thermal effect with an extrapolated temperature of 303.8°C is attributed to the thermolysis of the sample and evaporation of the decomposition products: its extreme at 324.2°C corresponds to the maximum rate of mass loss. The use of differentiation did not reveal the internal structure of the discussed thermal effect. The high-temperature region of the DSC curve contains an additional endothermic effect (with an extreme at 448.5°C) caused by the melting of Tl_2S (reference data: mp = 448.9°C [32]).

Two main steps of the mass loss can be distinguished in the TG curve of compound **II** (Fig. 9*a*). The first step (~200–290°C) is caused by the thermolysis of the complex simultaneously by the $[Au\{S_2CN(CH_2)_4O\}_2]^+$ cation (with gold(III) reduction to the elemental state) and $[TlCl_4]^-$ anion (with TlCl release). The inflection point at 245°C divides this region of the TG curve into two sections. The mass loss before the inflection point (28.13%) suggests

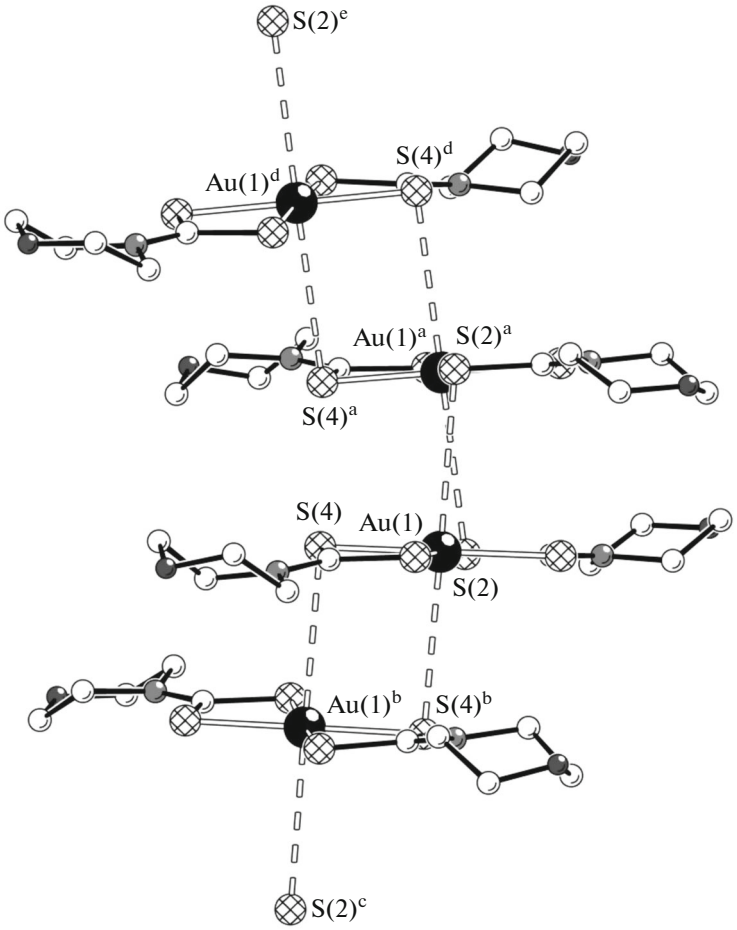

Fig. 7. Two-unit fragment of the cation-cationic polymeric helical chain $([Au_2\{S_2CN(CH_2)_4O\}_4]^{2+})_n$ oriented along the crystallographic axis *y*; secondary bonds Au···S are shown by dash. Symmetry codes: [a] $1/2 - x, 1 - y, z$; [b] $x, 1/2 - y, 3/2 - z$; [c] $1/2 - x, y - 1/2, 3/2 - z$; [d] $1/2 - x, 1/2 + y, 3/2 - z$; [e] $x, 3/2 - y, 3/2 - z$.

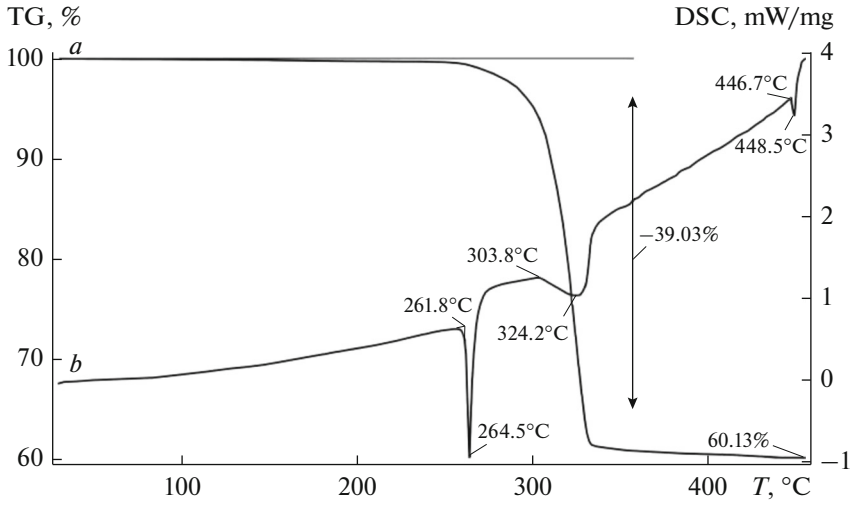

Fig. 8. (*a*) TG and (*b*) DSC curves for complex **I**.

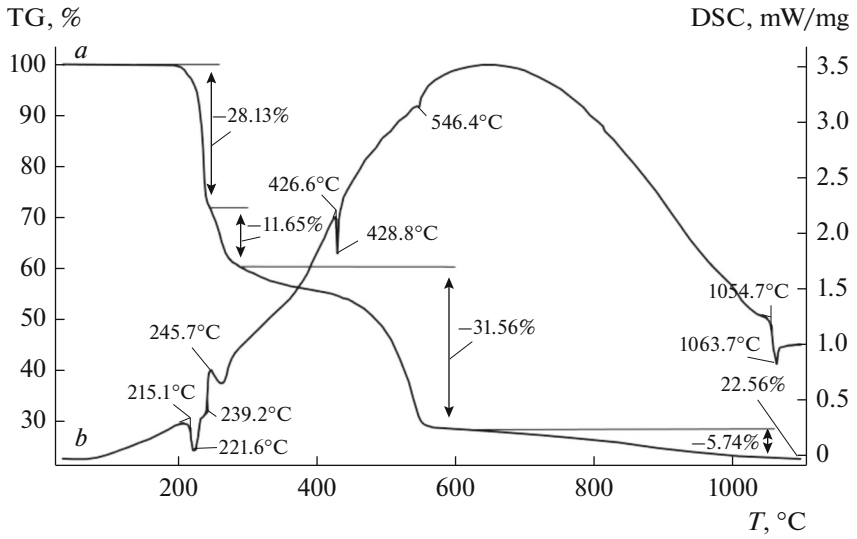

Fig. 9. (*a*) TG and (*b*) DSC curves for complex **II**.

that the initial stage of the thermal destruction of complex **II** is related to the elimination of two alkoxyl fragments $(=CHCH_2)_2O$ to form the intermediate cation $[Au(S_2CNH_2)_2]^+$ [33] and three chlorine atoms (calcd. 28.62%). Since the thermolysis of compound **II** starts at 200°C, $TlCl_3$ released by the anion begins to decompose already at the moment of release. According to published data [32], at the temperature higher than 150°C $TlCl_3$ decomposes to TlCl and chlorine.) The region of gold reduction to metal follows after 245°C (calcd. mass loss 21.24%) and is conjugated with the second step of the TG curve (mainly caused by the evaporation of TlCl, calcd. 27.64%) and subsequent reaching the smooth region of the final desorption of volatile thermolysis products. The total experimentally detected mass loss in three discussed regions of the TG curve is equal to 48.95% (11.65 + 31.56 + 5.74%), which completely corresponds to a total calculated value of 48.88% (21.24 + 27.64%). At the completion of the process at 1100°C, the weight of the residue is 22.56% of the initial value, which is close to the calculated value equal to 22.70% for reduced metallic gold.

The DSC curve in the low-temperature range shows two thermal effects: the endothermic effect with an extreme at 221.6°C and the exothermic effect at 245.7°C (Fig. 9*b*). The endothermic effect with an extrapolated temperature of 215.1°C is assigned to the melting of complex **II** with decomposition. For independent determination in a glass capillary, the unstable character of the sample (irreversible blackening) is detected at 215°C, whereas the melting with evident signs of decomposition falls on a range of 220–221°C. It is important to mention when discussing the nature of the exothermic effect that the latter is projected onto the first step of the TG curve corresponding to the thermolysis of compound **II** and is accompanied by the formation of TlCl. Since the second step of mass loss is mainly related to the evaporation of TlCl and the corresponding region of the DSC curve includes the endothermic effect of its melting with the extreme at 428.8°C (reference mp = 431°C [32]), it can be concluded that the discussed exothermic effect is due to the crystallization of the formed thallium(I) chloride. The weak endothermic effect with the extreme at 546.4°C is related to the evaporation of thallium(I) chloride. The endothermic effect with the extreme at 1063.7°C showing the melting of reduced gold is observed in the high-temperature section of the DSC curve.

ACKNOWLEDGMENTS

This work was supported in part by the Presidium of the Far East Branch of the Russian Academy of Sciences (program "Dal'nii Vostok," project no. 15-I-3-001).

REFERENCES

1. Riley, J.P. and Siddiqui, S.A., *Anal. Chim. Acta*, 1986, vol. 181, p. 117.
2. Elson, C.M. and Albuquerque, C.A.R., *Anal. Chim. Acta*, 1982, vol. 134, p. 393.
3. Nilson, L. and Hesse, R., *Acta Chem. Scand.*, 1963, vol. 23, no. 6, p. 1951.
4. Jennische, P., Olin, Å., and Hesse, R., *Acta Chem. Scand.*, 1972, vol. 26, no. 7, p. 2799.
5. Jennische, P. and Hesse, R., *Acta Chem. Scand.*, 1973, vol. 27, no. 9, p. 3531.
6. Anacker-Eickhoff, H., Jennische, P., and Hesse, R., *Acta Chem. Scand.*, Ser. A, 1975, vol. 29, no. 1, p. 51.

7. Pritzkow, H. and Jennische, P., *Acta Chem. Scand.*, Ser. A, 1975, vol. 29, no. 1, p. 60.
8. Elfwing, E., Anacker-Eickhoff, H., Jennische, P., and Hesse, R., *Acta Chem. Scand.*, Ser. A, 1976, vol. 30, no. 5, p. 335.
9. Hong, S.-H. and Jennische, P., *Acta Chem. Scand.*, Ser. A, 1978, vol. 32, no. 4, p. 313.
10. Alexander, N., Ramalingam, K., and Rizzoli, C., *Inorg. Chim. Acta*, 2011, vol. 365, no. 1, p. 480.
11. Akhbari, K. and Morsali, A., *Coord. Chem. Rev.*, 2010, vol. 254, nos 17–18, p. 1977.
12. Ramalingam, K., Rizzoli, C., and Alexander, N., *Monatsh. Chem.*, 2013, vol. 144, no. 9, p. 1329.
13. Sivagurunathan, G.S., Ramalingam, K., and Rizzoli, C., *Polyhedron*, 2013, vol. 65, p. 316.
14. Gomathi, G., Thirumaran, S., and Ciattini, S., *Polyhedron*, 2015, vol. 102, p. 424.
15. Kumar, V., Singh, V., Gupta, A.N., Drew, M.G.B., and Singh, N., *Dalton Trans.*, 2015, vol. 44, no. 4, p. 1716.
16. Ramalingam, K., Rizzoli, C., and Sivagurunathan, G.S., *New J. Chem.*, 2016, vol. 40, no. 3, p. 2489.
17. Manar, K.K., Rajput, G., Yadav, M.K., Yadav, C.L., Kumari, K., Drew, M.G.B., and Singh, N., *Chem. Select.*, 2016, vol. 1, no. 18, p. 5733.
18. Ivanov, A.V., Bredyuk, O.A., Gerasimenko, A.V., and Antzutkin, O.N., *Dokl. Phys. Chem.*, 2008, vol. 420, no. 2, p. 130.
19. Rodina, T.A., Ivanov, A.V., Bredyuk, O.A., and Gerasimenko, A.V., *Russ. J. Coord. Chem.*, 2009, vol. 35, no. 3, p. 170.
20. Ivanov, A.V., Bredyuk, O.A., Gerasimenko, A.V., et al., *Russ. J. Coord. Chem.*, 2006, vol. 32, no. 5, p. 339.
21. Ivanov, A.V., Bredyuk, O.A., Loseva, O.V., and Rodina, T.A., *Russ. J. Coord. Chem.*, 2015, vol. 41, no. 2, p. 108.
22. Ivanov, A.V., Bredyuk, O.A., Loseva, O.V., and Antzutkin, O.N., *Russ. J. Inorg. Chem.*, 2016, vol. 61, no. 6, p. 755.
23. Byr'ko, V.M. *Ditiokarbamaty*, Moscow: Nauka, 1984.
24. Pines, A., Gibby, M.G., and Waugh, J.S., *J. Chem. Phys.*, 1972, vol. 56, no. 4, p. 1776.
25. *Bruker, APEX2 (version 1.08), SAINT (version 7.03), SADABS (version 2.11), SHELXTL (version 6.12)*, Madison: Bruker AXS Inc., 2004.
26. *Khimicheskaya entsiklopediya* (*Chemical Encyclopedia*), Zefirov, N.S., Ed., Moscow: Bolshaya Rossiiskaya Entsiklopediya, 1995.
27. Pauling, L., *The Nature of the Chemical Bond and the Structure of Molecules and Crystals*, London: Cornell Univ., 1960.
28. Bondi, A., *J. Phys. Chem.*, 1964, vol. 68, no. 3, p. 441.
29. Bondi, A., *J. Phys. Chem.*, 1966, vol. 70, no. 9, p. 3006.
30. Alcock, N.W., *Adv. Inorg. Chem. Radiochem.*, 1972, vol. 15, no. 1, p. 1.
31. Urusov V.S. *Teoreticheskaya kristallokhimiya* (Theoretical Crystal Chemistry), Moscow: Izd. MGU, 1987.
32. Lidin, R.A., Molochko, V.A., and Andreeva, L.L. *Khimicheskie svoistva neorganicheskikh veshchestv* (Chemical Properties of Inorganic Substances) Moscow: Khimiya, 2000.
33. Ivanov, A.V., Loseva, O.V., Rodina, T.A., et al., *Russ. J. Coord. Chem.*, 2016, vol. 42, no. 2, p. 104.

Translated by E. Yablonskaya